Title

# Prediction of the thermal-hydraulic-mechanical response of a geological repository at large scale and sensitivity analyses



Authors
Guo, Ruiping
Xu, Hao
Plúa, Carlos
et al.

Publication Date
2020-12-01

DOI
10.1016/j.ijrmms.2020.104484

Peer reviewed

# Prediction of the thermal-hydraulic-mechanical response of a geological repository at large scale and sensitivity analyses

*Ruiping Guo[1], Hao Xu[2], Carlos Plua[3], Gilles Armand[3]*

*[1]Nuclear Waste Management Organization*

*[2]Lawrence Berkeley National Laboratory (LBNL), Berkeley, California, U.S.A.*

*[3]Andra R&D Division, Meuse/Haute-Marne URL, Bure, France*

## Abstract

To better understand the Thermal-Hydraulic-Mechanical (THM) response of the rock caused by the high-level radioactive waste (HLW) released heat in the Callovo-Oxfordian formation (COx) in the near-field and far-field areas, a series of coupled THM modelling is performed. This study presents a case study based on the French geological repository for HLW (Cigéo project) to better assess modelling of deep geological repositories (DGR) within the DECOVALEX-2019 framework. In this study, the proposed coupled THM model, implemented in the platform of COMSOL, is validated by comparing the modelled THM results for a point heat source in an infinite rock mass with an analytical solution. It is also validated by comparing its thermal component for the Base Case with accurate results calculated using another numerical method. To shorten the calculation time, the DGR is modelled using six cuboid blocks representing 162 HLW cells and only six central HLW cells of interest modelled in detail. This simplification is validated. This model can easily be used to model not only the near-field THM response of the rock but also the far-field THM response. The influence of the boundary conditions applied on the gallery wall, HLW cell walls, and model external surfaces and the influence of different vertical dimensions of the geometry are studied. The sensitivity analyses of the THM parameters of COx on the THM response at different locations are performed. The influence of

using a 2-dimensional (2D) model to represent a 3-dimensional (3D) repository is also investigated.

## 1. Introduction

Many countries using nuclear power for the production of electricity, including France, are currently considering the long-term disposal of their high-level radioactive wastes (HLW) in a deep repository located in a suitable geological formation, such as the Callovo-Oxfordian formation (COx). Geological disposal relies on multiple barriers – for example, engineered clay barriers and thick layers of natural sedimentary rocks – to contain and isolate the radioactive waste for a very long period of time.

The temperature increase caused by heat input from the radioactive waste can affect many aspects of near-field and far-field behaviour. For example, the heating and associated temperature variation can change the mechanical behaviour of the rock [1], and thermal expansion of both the solid rock constituents and the water in the rock pores can create a potential for increased rock damage near the underground openings and progressive rock failure [2]. Rock pore pressure changes induced by thermal expansion influence both the rock stresses and the hydraulic gradients. Increased pore pressure in the pores and microfractures of the rock will result in a reduction of normal effective stress, potentially leading to tensile fracturing or to unpredictable propagation of hydraulic fracture [3]. Non-uniform pore pressure increase will alter the existing hydraulic gradients and can affect both the quantity of flow through the rock and the flow direction, thus potentially affecting the advective transport of water-borne radionuclides [4]. Therefore, the long-term performance of these barriers is investigated collaboratively by interdisciplinary researchers.

In the current French concept, the HLW will be placed in a set of parallel micro-tunnels of 0.75 m to 0.80 m in diameter and 80 m to 150 m in length as shown in Figure 1 [5]. The HLW zone covers an area of around 8 km$^2$ of the geological formation of the COx in which the rock shows vertical and horizontal mineralogical variation and therefore, the thermal-hydraulic-mechanical (THM) properties are variable. COx claystone comprises a dominant clay fraction rich in carbonates, quartz, minor feldspars and accessory minerals. On average, the COx claystone contains 25-55 % clay minerals, 20-38% carbonates, 20-30% quartz, 1% feldspar, and small amount of others [6]. The sedimentation has caused a preferential orientation of the clay formation and consequently a stratification of the matrix structure. This results in anisotropy of the rock properties. An anisotropic behaviour is found in the COx based on the mechanical tests performed on the samples obtained following different orientations. The parallel to bedding stiffness of the COx is greater than its perpendicular to bedding stiffness. Horizontal thermal conductivity (i.e., parallel to the bedding) of the COx is also higher than the vertical one. Concerning the water permeability, a slight anisotropy ratio of horizontal to vertical between 2 and 3 is observed. Regarding in situ stress, an anisotropy is also observed. The largest principal stress is horizontal and the vertical and the smallest horizontal stresses are similar in magnitude [7]. At the main level of the Meuse/Haute-Marne Underground Research Laboratory (MHM URL) (i.e., at -490 m) the maximum stress, which is parallel to the direction of the heater boreholes, is about 16 MPa and both the middle (vertical stress) and the minor stresses are about 12 MPa. The hydraulic and mechanical response is also influenced by the orientation of the in situ stress directions [5, 8-10].

To better understand the THM response caused by the radioactive waste released heat in the COx formation for the near-field and far-field areas of the HLW cells, a series of 2D or 3D coupled THM modelling is performed. This study has been conducted in Task E within the DECOVALEX-2019 framework, an international program with a 4-year duration that started in 2016. DECOVALEX is a multidisciplinary, co-operative international research effort in modelling coupled Thermal-Hydraulic-Mechanical-Chemical (THMC) processes in geological systems and addressing their role in Performance Assessment for radioactive waste storage [11]. One of the goals of Task E is to propose guidelines for repository-scale calculations for a deep repository in the COx formation by assessing the effect of choice of THM modelling [12-13]. The numerical simulation of a deep repository is a case study based on the French geological repository for high-level radioactive waste, Cigéo project. The data was provided by the French National Agency for Radioactive Waste Management (Andra) leading Task E. Calculations presented in the following sections are not part of the design of the real project.

Considerable effort has been expended in numerical modelling and interpretation of experimental results related to coupled THM processes to understand the mechanism of the coupling process [14-21]. These studies focused on interpretation of the THM response of in-room or in-situ experiments. A series of conceptual design studies for a DGR was also carried out in the past [22-33]. These studies include two and three-dimensional thermal transient and thermo-mechanical analyses. Because it is not numerically practical to include near-field details in a repository size model, these analyses are typically divided into near-field and far-field modelling. The near-field model includes a unit cell geometry from a repository with an adiabatic thermal condition, no hydraulic flow and roller mechanical boundary condition applied on the four vertical external boundaries and as such, this represents a repository with an infinite horizontal dimension. The purpose of a near-field model is to study the THM responses of engineered or natural sealing materials, for example, nuclear waste container temperature, clay-based buffer material saturation, or stability of the rock surrounding the placement room. However, for a finite dimension repository, results generated with this approach are accurate for early times with the thermal response overestimated at longer times [33]. To correct for this, a method was proposed by Guo [33] to modify near-field thermal results, but the method cannot be used to solve hydraulic and mechanical response. In this study, a coupled THM model is proposed in which both far-field geometry of a DGR and near-field details at the location of interest are incorporated.

## 2 Coupled THM theory

### *2.1 Thermal equations*

To simplify the modelling, thermal radiation is not considered. The following thermal equation is used for thermal modelling [34]:

$$c_p \rho \frac{\partial T}{\partial t} + \rho_w c_{pw} \boldsymbol{v} \cdot \nabla \mathrm{T} + \nabla \cdot \mathbf{q} = Q \quad (1)$$

where $T$ is temperature (ºC), $t$ is time (s), $\rho$ is bulk density (kg/m$^3$), $c_p$ is equivalent specific heat capacity of the porous matrix (J/(kg·ºC)), $Q$ is a specific source of heat (W/m$^3$), $c_{pw}$ is specific heat capacity of water (J/(kg·ºC)), $\boldsymbol{v}$ is Darcy's velocity (m/s), and $\mathbf{q}$ is the heat flux (W/m$^2$), which can be defined as follows [34]:

$$\mathbf{q} = -\boldsymbol{\lambda} \nabla T \quad (2)$$

where $\boldsymbol{\lambda}$ is the thermal conductivity tensor (W/(m·ºC)).

In Equation (1), $\rho_w$ is the density of water (kg/m$^3$), which is a function of temperature and pore pressure and can be linearly expressed as follows [35]:

$$\rho_w = \rho_0 (1 + \beta (p - p_0) - \alpha_w (T - T_0)) \quad (3)$$

where $\rho_0$ is the density of water at reference pressure and reference temperature (kg/m$^3$), β is the water compressibility (1/Pa), $\alpha_w$ is the water volumetric thermal expansion coefficient (1/ºC), $p$ is the pore pressure (Pa), $p_0$ is the reference pressure (Pa), and $T_0$ is the reference temperature (ºC).

### 2.2 Hydraulic equations

Water balance equation is used for the coupled model as follows:

$$\frac{\partial(\phi\rho_w)}{\partial t} + \phi\rho_w \frac{1}{1+\varepsilon_v} \frac{\partial\varepsilon_v}{\partial t} - \nabla\cdot\left(\rho_w \frac{k}{\mu}(\nabla p - \rho_w \boldsymbol{g})\right) = 0 \qquad (4)$$

where $\boldsymbol{g}$ is the vector of gravity (m/s$^2$), $k$ is permeability tensor (m$^2$), $\varepsilon_v$ is the volumetric strain (unitless), and $\mu$ is viscosity (Pa·s) , which is a function of temperature and can be expressed as follows [36]:

$$\mu = Aexp(\frac{B}{273+T}) \qquad (5)$$

where $A$ is a constant (Pa·s), and $B$ is an exponential constant (ºC).

In Eq. (4), $\phi$ is porosity (unitless), which is a function of temperature, pore pressure and volumetric strain and can be expressed as follows:

$$\phi = (\phi_0 + \alpha_B\varepsilon_v + (\alpha_B - \phi_0)(p - p_0)(1 - \alpha_B)C_m - \alpha_s(\alpha_B - \phi_0)(T - T_0))/(1 + \varepsilon_v) \qquad (6)$$

where $\phi_0$ is the initial porosity (unitless), $\alpha_s$ is the volumetric thermal expansion coefficient of the rock (1/ºC), $C_m$ is the compressibility of the solid phase (Pa$^{-1}$), and $\alpha_B$ is the Biot coefficient (unitless).

### 2.3 Mechanical equations

In this exercise, the COx is assumed to be an elastic material. The following equation is used for the mechanical response of the COx, including hydraulic and thermal effects [37]:

$$\rho \frac{\partial^2 \boldsymbol{u}}{\partial t^2} - \nabla \cdot \boldsymbol{\sigma} = \boldsymbol{F}_v \tag{7}$$

where $\boldsymbol{u}$ is the displacement vector, $\boldsymbol{F}_v$ is the body force, $\boldsymbol{\sigma}$ is the total stress tensor (negative is compressive stress in this equation). Thermal and hydraulic processes are coupled to the mechanical equations through addition of a stress term for pore pressure ($\boldsymbol{\sigma}_{ext}$, which is the external stress and is equal to $-\alpha_B p\bar{\boldsymbol{I}}$) and addition of a strain term for thermal expansion such that stress - strain relationship becomes:

$$\boldsymbol{\sigma} - \alpha_B p \bar{\boldsymbol{I}} = \bar{\mathbf{C}}: (\boldsymbol{\varepsilon} - \boldsymbol{\varepsilon}_T) \tag{8}$$

where $\bar{\boldsymbol{I}}$ is a 3x3 identity tensor, $\boldsymbol{\varepsilon}$ is the strain tensor, $\bar{\mathbf{C}}$ is the 4$^{th}$ order elasticity tensor, ":" stands for the double-dot tensor product (or double contraction), and $\boldsymbol{\varepsilon}_T$ is the strain due to thermal expansion and can be calculated using the following equation:

$$\boldsymbol{\varepsilon}_T = \frac{\alpha_s}{3}(T - T_0)\bar{\boldsymbol{I}} \tag{9}$$

The strain is calculated using the following equation:

$$\boldsymbol{\varepsilon} = \frac{1}{2}[(\nabla \boldsymbol{u})^T + \nabla \boldsymbol{u}] \tag{10}$$

### *2.4 Implementation of the coupled THM theory in COMSOL*

The mathematical equations described above have been implemented in the finite element code COMSOL. In COMSOL, a fully coupled approach can be implemented to solve all set of equations for thermal, mechanical, and single/multiphase flow in the same simulator (COMSOL). The fully coupled approach forms a single large system of equations that solve for all of the unknowns and includes all of the couplings between the unknowns at once within a single iteration. A Newton-Raphson iteration scheme for non-linear problems with the MUMPS direct solver for the linear updates is used in this fully coupled approach. Backward differentiation formula (BDF) dynamic time-stepping is used but with a cap (e.g., a cap time step size of $1 \times 10^{10}$ s is used in Sections 3) to ensure time steps do not span multiple output times.

# 3. Coupled THM COMSOL model

## *3.1 Three-dimensional COMSOL model*

### *3.1.1 Model geometry*

Figure 2 shows the geometry of the three-dimensional COMSOL model of a Base Case for the coupled THM simulation of a deep geological repository in the COx formation in France. The model geometry dimensions are 2.5 km x 2.0 km x 3.0 km including one quarter of a DGR considering symmetric conditions. It includes one connection gallery and 3 access galleries leading to 28 HLW cells at each side. There are 168 HLW cells in total with a cell-to-cell distance of 52.3 m, 162 of which are approximated using cuboid blocks to simplify the model. The other six central HLW cells are modelled in detail with individual micro-tunnels resolved in the model (Figure 2). The proposed configuration is a case representative of a quarter of a HLW repository for investigation purposes.

The COx formation is surrounded by the Dogger and Oxfordian limestone layers and it can be vertically divided into three unit layers: the Clay unit (UA), the Transition unit (UT), and the Silty Carbonate-Rich unit (USC). These three units differ in terms of mineralogical composition [6]. In total, eight geological layers are considered in this model. The depths of the different geological units and their abbreviations are shown in Table 1 [13].

Modelling results are output at three locations, which are represented as Points P1, P2 and P3 shown in Figure 2. P1 is centrally located between the third HLW Cell and the fourth HLW Cell, P2 is 2 m from the centre of the third HLW Cell and P3 is on the ground surface above P1.

### *3.1.2 Initial conditions for the Base Case*

The excavation of the access/connection tunnels is simulated and the results from the simulation of the access/connection tunnels are considered as the initial conditions for the HLW cell excavation stage and the results from the HLW cell excavation stage are considered as the initial conditions for the heating stage. The analyses focus on the last two stages. The time between the excavation of the access/connection tunnels and the HLW cell excavation is fixed to 10 years. The HLW cell excavation occurs at year 0 in the modelling. The HLW packages are emplaced inside the HLW cells two years later.

The initial temperature, initial pore pressure and initial stresses for the simulation of excavation of the access/connection tunnels at t = -10 years are functions of depth from the ground surface as shown in Figure 3. The initial stress is geostatic and isotropic in the Barrois, limestone and Kimmeridgian layers and anisotropic for the rest of them. The anisotropy ratio varies with depth from 1 to 1.3 in the Carbonated Oxfordian layer and it remains constant for the lower layers.

### *3.1.3 Boundary conditions for the Base Case*

The temperature on the top surface (Plane O′A′B′C′), the bottom surface (Plane OABC), the back surface (Plane CBB′C′) and the right surface (Plane AA′B′B) is also a function of depth from the ground surface as shown in Figure 3(a). Adiabatic condition is applied on the left surface (Plane OO′C′C) and the front surface (Plane OO′A′A) assuming that only one quarter of the entire repository is modelled (i.e., the planes OO′C′C and OO′A′A are symmetric surfaces). The heat power applied per meter HLW cell as a function of time is shown in Figure 4 [13].

The pore pressure on the top surface, the bottom surface, the back surface (Plane BB′C′C) and the right surface (Plane AA′B′B) is a function of depth from the ground surface as shown in Figure 3(b). No hydraulic flow is assumed to cross the left surface and the front surface assuming they are symmetric surfaces given that a DGR site chosen has a very slow hydrogeological flow.

The top surface is a mechanical free surface. A normal total stress $\sigma_x$ which is a function of depth as shown in Figure 3(c) is applied on the right surface (Plane AA′B′B). A normal total stress $\sigma_y$ which is also a function of depth as shown in Figure 3(c) is applied on the back surface (Plane CBB′C′). A roller boundary condition is applied on the left, front and bottom surfaces.

Boundary conditions of the HLW cells and the access tunnel during the last two stages of the simulations are shown in Table 2 [13].

#### *3.1.4 Material parameters*

Table 3 shows the minimum, mean and maximum values of the THM parameters of each layer in the vertical direction used for the simulation and these parameters are defined by DECOVALEX-2019 Task E [13]. In the Base Case modelling, the mean values are used. Table 4 shows the horizontal to vertical ratios of each parameter in the horizontal direction against its corresponding value in the vertical direction and they are defined by DECOVALEX-2019 Task E [13].

### *3.2 Two-dimensional COMSOL model for the Base Case*

Coupled THM 3-dimensional (3D) modelling typically requires a significant execution time. To understand whether a 2-dimensional (2D) model (plane strain) can be used (instead of a 3D model) to help understand the THM response in a deep geological repository, an analysis is also performed using a 2D Base Case model using the same parameters, same initial conditions and same boundary conditions as those used in the 3D Base Case model. The 2D model is a vertical cross section of geometry shown in Figure 2 through Points P1, P2 and P3.

# 4. Modelling results

## *4.1 Base Case modelling*

### *4.1.1 THM modelling results from the Base Case*

This section describes the modelling results related to the Base Case. In the Base Case, the mean values of the THM parameters are used except for Biot coefficient for which the minimum value (0.6) is used.

Figure 5 compares the temperatures at locations of Points P1 and P2 between the 2D model and the 3D model. There is no obvious difference between the 2D model and the 3D model during the first 100 heating years. After 100 years, the 2D model overestimates the temperatures at different locations. The maximum observed difference between the 2D model and the 3D model is less than about 3ºC at any location after 700 years. The peak temperatures at P2 and P1 are 59ºC after 29.7 years and 44ºC after 387 years from the 3D model, respectively.

Figure 6 compares the pore pressures at Points P1 and P2 between the 2D model and the 3D model. There is no difference in pore pressure during the first 40 years. After 40 years, at different locations, the 2D model greatly overestimates the pore pressure. The maximum observed difference between the 2D model and 3D model is about 3.7 MPa (51%) at Points P1 and P2 and occurs at 500 years. However, the difference between the maximum values obtained using 2D model and using 3D model is about 1.7 MPa which is an increase of about 13.8% (i.e., (14 MPa-12.3 MPa)/12.3 MPa). The peak pore pressures are 12.0 MPa at Point 2 after 40 years and 12.3 MPa at Point P1 after 38 years from the 3D model.

Figure 7 compares the uplifts at Point P3 between the 2D model and the 3D model. The 2D model greatly overestimates the uplift at the ground surface (P3). The peak value is 15.7 cm from the 2D model against 9.6 cm from the 3D model. Therefore, the 2D model overestimates the ground surface uplift about 64%.

The 2D model stands for a repository with infinite horizontal dimension in the Y-direction (see Figure 2 for direction). There are no thermal and hydraulic flux and no horizontal movement in the out-of-plane direction, thus the results from the 2D model greatly overestimate the THM response of rock caused by the heat in a finite DGR. Therefore, a 2D model cannot be used to accurately model the THM response in a DGR and surrounding rock in reality.

Figure 8 shows the simulated uplifts on the ground surface along O′A′ (for location see Figure 2) at four different times (100 years, 1000 years, 1580 years and 10000 years) obtained using 3D model. The uplift above the repository area is comparatively uniform at different times. The results shows that the uplift slope on the ground surface caused by existence of a DGR is less than 0.01% at anywhere on the ground surface.

Figure 9 shows the simulated stresses (positive is compressive) (a) in the X-direction and (b) in the Z-direction at Points P1 and P2 using the 3D model, respectively. Due to thermal expansion, the horizontal stress increases in the X-direction are about 4.5 MPa after 40 years at Point 2 and 4.6 MPa after 750 years at Point P1. Due to the vertical thermal expansion of the rock near the HLW cell wall greater than that at Point P1, the vertical stress decreases about 3.8 MPa at 40 years and later the thermal load decrease causes the decrease in thermal contraction in the surrounding rock, which, in turn, results in increase in the vertical stress at P1. At Point P2, the vertical stress increases at the first two years due to the adjacent HLW cell excavation and then decreases until 120 years and thereafter increase for the same reason as for the location of P1.

In summary, the temperatures reach peak values of 59ºC at Point P2 at Year 29.7 and 44ºC at mid-point (P1) between two HLW cells at Year 387. The pore pressures are 12.0 MPa at Point

P2 after 40 years and 12.3 MPa at Point P1 after 38 years. The simulated uplift on the ground surface above Point P1 reaches its peak value of 9.6 cm after 1570 years. Due to thermal expansion, the horizontal stress in the X-direction increases about 4.6 MPa at Point P1 and 4.5 MPa at Point P2 after about 750 years, while vertical stress at Point P1 decreases about 3.8 MPa.

The 2D model significantly overestimates the THM response of a deep geological repository. The thermal results between the 2D and the 3D models are found to have the best agreement within the first 100 years, the hydraulic results have a good agreement within the first 40 years, and the uplifts on the ground surface have a good agreement within the first 10 years. Maximum observed overestimations by the 2D are found to be 7% for temperature, 51% for pore pressure and 64% for the ground surface uplift.

#### *4.1.2. Validation of geometrical simplifications*

To shorten the calculation time, in the 3D model, the repository is simplified as six blocks with only six central HLW cells incorporated in detail. How the results may be affected by this simplification is studied. Reducing the number of HLW cells incorporated in detail to four or two has a very slight influence on the numerical results regardless the location of the studied points as shown in Figure 10. Increasing the number of HLW cells incorporated in detail to eight has no influence on the temperature and the pore pressure at different points. Similar conclusions are obtained in terms of the effective stress. These results validate the simplification, which reduces the computational cost of modelling a full HLW repository. This validation exercise is also done under plane-strain conditions by comparing a simplified model with six central HLW cells and blocks against a detailed geometry model.

#### *4.1.3 Influence of different boundary conditions*

##### *4.1.3.1 Influence of the galley wall boundary conditions*

Figure 11 shows the Influence of filling access/connection tunnels with fully-saturated buffer (a) after 2 years and (b) after 1000 years instead of applying atmospheric boundary condition on the gallery wall on the pore pressure at Points P1 and P2. Assuming the galleries are filled with fully saturated buffer materials after two years does not have any influence for the first 60 years but later greatly overestimates pore pressures at both Points P1 and P2. Assuming the galleries are filled with buffer materials fully saturated after 1000 years does not have any influence on modelling results but overestimates pore pressures after 1000 years at both Points P1 and P2. Both cases do not affect the peak pore pressure. Similar conclusions are obtained in terms of the effective stress.

Figure 12 shows the influence of assuming the buffer materials in galleries are fully saturated after two years and after 1000 years on the uplift at Point P3. Assuming the galleries are filled with fully saturated buffer material after two years overestimates the peak uplift about 14%. Assuming the galleries are filled with buffer materials fully saturated after 1000 years overestimates peak value about 6%. Therefore, estimation of the time for the filling material in access/connection tunnels reaching fully saturated is very important for the boundary condition setting in this kind of modelling.

*4.1.3.2 Influence of the HLW cell wall boundary conditions*

Figure 13 shows the influence of using fixed boundary condition on the HLW cell wall (representing the steel casing used for containing HLW) instead of free boundary condition used in the Base Case on the pore pressure at Points P1 and P2. There is no noticeable influence on the pore pressure at P1 and P2. Similar conclusions are obtained in terms of the effective stress and uplift on the ground surface. This indicates that the HLW cell boundary conditions can only influence the very small zone near the HLW cell wall.

*4.1.3.3 Influence of the model vertical dimension and other boundary conditions*

Influence of the model vertical dimensions (e.g., 1135 m, 1635 m, or 2635 m) is studied and the results show only the ground surface uplift is affected by the vertical dimensions of the repository domain [38]. There is no obvious difference in the uplift between the model with a vertical dimension of 2635 m and the Base Case which has a vertical dimension of 3000 m, but, with smaller dimensions (e.g., 1135 m or 1635 m), the uplift is underestimated because the thermal expansion of the rock within the depth range of 1135 m to 2635 m is not considered. However, no change in numerical results of the temperature, pore pressure and effective stresses is observed.

The following cases are also studied to investigate the influence of boundary conditions applied on the external boundary surface in Figure 2 [38]:

- The influence of using fixed pore pressure boundary condition on the model bottom surface instead of no-flow boundary condition used in the Base Case on the pore pressure at Point P1 and P2.
- The influence of using no heat flow boundary condition on the front and right side vertical surfaces of the model instead of using fixed temperature boundary condition used in the Base Case on the temperature and pore pressure at Points P1 and P2.

Due to the dimensions being large enough, no differences are observed for both cases compared with the Base Case results suggesting model boundary conditions are not driving model results.

In summary, model results are not sensitive to exterior model hydraulic, or thermal, or mechanical boundary conditions. This indicates that the model domain (2 km x 2.5 km x 3 km) is appropriate to perform the coupled THM modelling. The boundary conditions on the gallery wall have influence on the pore pressure but do not influence the peak value. Assuming the galleries are filled with fully saturated buffer materials after two years overestimates the ground surface uplift 14%. Using fixed or free boundary condition on the HLW cell wall does not influence the analysis of the pore pressure at the selected locations.

### *4.2 Parameter sensitivity analyses*

In this section, the influence of the different THM parameters on the THM responses is studied using the 3D model. It includes the influence of the minimum or maximum values of each THM parameter used for all layers of USC, UT, UA23 and UA1, the minimum values of hydraulic permeability of each single sublayer of COx, the minimum values of thermal conductivity of each single sublayer of COx, and the maximum values of Young's modulus of each single sublayer of COx.

#### *4.2.1 Sensitivity analyses of THM parameters of COx including USC, UT, UA23 and UA1*

The influence of all THM parameters on the temperature at P2 is studied, but only the minimum thermal conductivity, minimum specific heat capacity, and minimum equivalent density of rock of Layers USC, UT, UA23 and UA1 have influence on the temperature increase at P2 as shown in Figure 14. The minimum values of thermal conductivity of Layers USC (a decrease of 28%), UT (27%), UA23 (25%) and UA1 (31%) cause peak value increase of temperature at P2 of 6ºC (from 59ºC to 64.8ºC).

The influence of all THM parameters of Layers USC, UT, UA23 and UA1 on the pore pressures at P2 is studied. Only minimum permeability, the minimum thermal conductivity, the maximum porosity, maximum Young's modulus, and minimum specific heat capacity have obvious influence on increasing pore pressure at P2 as shown in Figure 15. The minimum permeability (a decrease of 86%) of Layers USC, UT, UA23 and UA1 causes the peak value of pore pressure to increase from 11.9 MPa at 40 years to 16.6 MPa at 6 years (about increase 40%).

Figure 16 shows the influence of the minimum permeability, the minimum thermal conductivity, minimum Young's modulus, minimum specific heat capacity, maximum Poisson's ratio, maximum Biot coefficient, and maximum thermal expansion of Layers USC, UT, UA23 and UA1 on the uplift at P3. All these parameter values cause the uplift at P3 to increase. The minimum permeability (a decrease of 86%) of Layers USC, UT, UA23 and UA1 causes the peak value of the uplift to increase from 9.6 cm at 1570 years to 12.9 at 780 year (about increase 34%).

In summary, the three major factors influencing temperatures are thermal conductivity, specific heat capacity and equivalent density with the most important factor being thermal conductivity. Assuming a minimum value for thermal conductivity results in a maximum temperature overestimation of 8.5ºC in the rock near the HLW cell.

The major significant five factors influencing the pore pressure are permeability, thermal conductivity, porosity, Young's modulus, and specific heat capacity with the most important factor being permeability. Assuming a minimum value for permeability (a decrease of 86%) results in a maximum pore pressure overestimation at P2 by 40%.

The major significant five factors influencing the ground surface uplift are permeability, thermal expansion, Young's modulus, Poisson's ratio, and Biot coefficient, with the most important factor being permeability. Assuming a minimum value for permeability (a decrease of 86%) results in a maximum uplift overestimation at the ground surface by 34%.

#### *4.2.2 Sensitivity analyses of parameters of a single sublayer rock of COx*

##### *4.2.2.1 Influence of minimum permeability values of Layer UA23, or UA1, or UT, or USC used on the THM response*

Figure 17 shows the influence of the minimum permeability values of Layer UT, or UA1, or UA23 or USC used in the COMSOL model on the pore pressure at Points P1 and P2. Although there are some influences of the minimum permeability values of Layer UT, or UA1, or USC used on the pore pressure at later time (after 100 years), there is no influence on the pore pressure peak value. However, the influence of the minimum permeability value of Layer UA23 (a decrease of 86%) is significant and it can cause overestimation of the peak pore pressure 27% at Point P1 and 39% at Point2.

*4.2.2.2 Influence of minimum thermal conductivity values of Layer UA23, or UA1, or UT, or USC used on the THM response*

Figure 18 shows the influence of the minimum thermal conductivity values of Layer UA23, or UT, or UA1, or USC used in the COMSOL model on (a) temperature and (b) pore pressure at Points P1 and P2. The influences of the minimum thermal conductivity values of Layer UT, or UA1 or USC on the temperature or on the pore pressure at different locations are very minor, because these layers are far away from the repository. The thermal conductivity of Layer UA23 has a significant influence on the temperatures and on the pore pressures at Points P1 and P2. Using the minimum thermal conductivity of Layer UA23 (a decrease of 25%) can cause 13% overestimation of the peak temperature at Point P2.

*4.2.2.3 Influence of maximum Young's Modulus values of Layer UA23, or UA1, or UT, or USC used on the THM response*

Figure 19 shows the influence of the maximum Young's modulus of Layer UA23, or UA1, or UT, or USC used in the COMSOL model on the pore pressure at Point P1 and Point P2. There is no influence of using maximum Young's modulus values of Layer UA1, or UT, or USC instead of using the mean value on the pore pressure. But using the maximum value of the Young's modulus of Layer UA23 (an increase of 52%) can overestimate 7% of the peak value of the pore pressure.

In summary, the major factors influencing the THM responses of the deep geological repository are the THM parameters of Layer UA23 which hosts the deep geological repository. The THM parameters in the layers above or below Layer UA23 do have an influence on the THM responses but the influence is very minor because they are far away from the DGR.

## *5.* Validation

There are no available direct theoretical solution or physical test results for this model at this moment. To validate this model, two steps are taken. The first step is to validate the coupled THM model implemented in COMSOL by comparing the THM response in an infinite rock mass with a point heat source using a theoretical solution [39-40]. The second step is to validate the coupled THM model for the HLW repository by comparing the thermal components from the Base Case calculation with the calculated results from Guo [33], which can provide accurate thermal results for a deep geological repository.

### *5.1 Validation of the coupled THM model*

When a point heat source is buried in a saturated soil, the temperature changes that occur will cause the pore water to expand a greater amount than the voids of the soil. If the soil is sufficiently permeable these pore pressures will dissipate. Smith and Booker [39] developed an analytical solution for a linear theory of thermo-poroelastic consolidation in a homogeneous isotropic material.

In the calculation for comparison, the dimensions of a 3D COMSOL model built are 15 m x 15 m x 15 m as shown in Figure 20. The initial temperature, initial pore pressure and initial stresses are set to 0°C, 0 MPa, and 0 MPa. The three symmetric planes (x = 0 m, y = 0 m, and z = 0 m, see Figure 20 for location) are defined as impermeable and adiabatic. At external model boundaries (x = 15 m, y = 15 m, and z = 15 m), the temperature and pore pressure are set to 0°C and 0 Pa. A constant point power of Q = 700 W is applied at point (0, 0, 0). Regarding mechanical conditions, all boundaries are free except the symmetric planes (x= 0 m, y = 0 m, and z = 0 m) where a roller boundary condition is applied.

For the purpose of validation, the material in the packer borehole is assumed to be rock material. The rock and water parameters used are as shown in Table 5.

The modelled temperatures, pore pressures, displacements and normal stresses at Points Q1 (0.35, 0, 0), Q2 (0.5, 0, 0), Q3 (1.5, 0, 0) and Q4 (0.35, 0.5, 0.6) are compared with the theoretical solutions below.

Figure 21 compares the simulated (a) temperatures and (b) pore pressures using the COMSOL model with the analytical solutions at Points Q1, Q2, Q3 and Q4 and Figure 22 compares the simulated (a) displacements and (b) normal stresses using the COMSOL model with the theoretical solutions at Point Q4, respectively. The calculated results match the theoretical solution exactly. This indicates that the coupled THM model used in this paper can be used to correctly model the THM response in a fully saturated poroelastic material.

In summary, the excellent agreement between the numerical model and the analytical solutions indicates that the proposed coupled model can be used to simulate coupled THM processes in a fully saturated geotechnical material.

### *5.2 Validation of the 3D COMSOL model*

In this study, only six HLW cells are incorporated in detail to simplify the model and reduce the calculation time. The accuracy of this coupled THM model and the simplification used in this model need to be validated. Guo [33] proposed a method which can calculate accurate temperatures at any locations in a deep geological repository. In Guo [33], a near-field thermal modelling is performed to predict the thermal response in the near-field area from a horizontally infinite DGR. By subtracting the thermal response caused by the heat load beyond the finite DGR area from the near-field modelling results, the true thermal response in the near-field area is obtained for a finite DGR.

To validate the coupled THM COMSOL model, the temperatures at Points P1 and P2 calculated using the method proposed in Guo [33] are compared with the thermal components of the coupled THM model results of the Base Case as shown in Figure 23. The excellent agreement in the temperature comparison indicates that the coupled THM model in Section 3 is correctly built.

## 6. Conclusions

A fully coupled THM 3D model is successfully implemented in the platform of COMSOL. This model is simplified by using cuboid blocks to represent the HLW cells with only six central HLW cells of interest modelled in detail. This simplification makes the model be easily used to model not only far-field THM response of a DGR but also the near-field THM response of the rock near HLW cells. The coupled THM model is initially validated by comparing the modelled THM results for a point heat load in an infinite rock mass with the analytical solution. It is also validated by comparing its thermal component for the Base Case with accurate results calculated using another numerical method. Using this model, a series of 2D or 3D coupled THM modelling has been performed to gain a better understanding of the thermal, hydraulic and mechanical responses in the near-field and far-field areas of case studies based on some data from the Cigéo project.

The modelling results for the Base Case of the 3D model show:

- The temperature at Point P2 reaches its peak of 59ºC after 29.7 years; and the temperature at mid-point (Point P1) between two HLW cells reaches its peak 44ºC after 387 years;
- The peak pore pressures are 12.0 MPa at Point P2 after 40 years and 12.3 MPa at Point P1 after 38 years;
- The simulated uplift on the ground surface above Point P1 reaches its peak of 9.6 cm after 1570 years; and
- The ground surface slop change caused by the DGR existence is less than 0.01%.

The thermal results from 2D and 3D models are found to have the best agreement within the first 100 years. The hydraulic results have a good agreement within the first 40 years and the mechanical results also have a good agreement within 40 years. Maximum observed temperature difference is 3ºC at different locations and occurs at 700 years, maximum observed pore pressure difference is 3.7 MPa at both Point P1 and Point P2 and occurs at 500 years, and maximum observed ground surface uplift difference is 6.1 cm (an increase of 64%). The 2D model represents a DGR with an infinite length of the HLW cells. Therefore, the 2D model is only appropriate for early stage after the waste emplacement and it overestimates the long-term THM responses of the DGR due to the null flux and no horizontal movement in the out-of-plane direction.

Assuming the buffer materials in the galleries is fully saturated after 1000 year only slightly influences pore pressure and ground surface uplift after 1000 years. Assuming the galleries are filled with fully saturated buffer materials after 2 years can cause pore pressure to increase only after 60 years but does not influence the peak value.

Applying the fixed mechanical boundary condition on the HLW cell walls does not significantly influence the analysis of the pore pressure at P1 and P2.

An importance ranking of all THM parameter is presented for the temperature, pore pressure and uplift in which the most important parameters are thermal conductivity, permeability and thermal expansion. The most important factor influencing temperature is thermal conductivity. The most important factor influencing pore pressure is rock permeability. The most important factors influencing the ground surface uplift are rock permeability and rock thermal expansion.

The influences of the THM parameters of the rock above or below Layer UA23 on the THM response in near-field or far-field results are very minor.

**Acknowledgements**

*DECOVALEX is an international research project comprising participants from industry, government and academia, focusing on development of understanding, models and codes in complex coupled problems in sub-surface geological and engineering applications; DECOVALEX-2019 is the current phase of the project. The authors appreciate and thank the DECOVALEX-2019 Funding Organisations Andra, BGR/UFZ, CNSC, US DOE, ENSI, JAEA, IRSN, KAERI, NWMO, RWM, SÚRAO, SSM and Taipower for their financial and technical support of the work described in this report. The statements made in the report are, however, solely those of the authors and do not necessarily reflect those of the Funding Organisations.*

## References

[1] Ranjith PG, Viete DR, Chen BJ, Perera MSA. Transformation plasticity and the effect of temperature on the mechanical behaviour of Hawkesbury sandstone at atmospheric pressure. Eng Geol 2012; 151: 120–127.

[2] Read RS, Martino JB, Dzik EJ, Oliver S, Falls S, Young RP. Analysis and interpretation of AECL's heated failure tests. Ontario Hydro, Nuclear Waste Management Division 06819-REP-01200-0070-R00. 1998.

[3] Berchenko I, Detournay E, Chandler N. Propagation of natural hydraulic fractures. Int J Rock Mech Min Sci 1997; 34 (3/4) (Paper no. 63).

[4] Dixon DA, Chandler NA, Graham J; Gray MN. Two large-scale sealing tests conducted at Atomic Energy of Canada Limited's Underground Research Laboratory: the Buffer/Container Experiment and the Isothermal Test. Can Geotech J 2002; 39: 503-518.

[5] Armand G, Bumbieler F, Conil N, de la Vaissière R, Bosgiraud JM Vu MN. Main outcomes from in situ thermo-hydro-mechanical experiments programme to demonstrate

feasibility of radioactive high-level waste disposal in the Callovo-Oxfordian claystone. J Rock Mech Geotech Eng 2017; 9: 415-427.

[6] Andra. Synthesis – Evaluation of the feasibility of a geo-logical repository in an argillaceous formation. DOSSIER 2005 Argile, 2005.

[7] Wileveau Y, Cornet FH, Desroches J, Blumling P. Complete in situ stress determination in an argillite sedimentary formation. Phys Chem 2007; 32: 866-878.

[8] Armand G, Noiret A, Zghondi J, Seyedi DM. Short- and long-term behaviours of drifts in the Callovo-Oxfordian claystine at the Meuse/Haute-Marne Underground Research Laboratory. J Rock Mech Geotech Eng 2013; 5: 221-230.

[9] Armand G, Leveau F, Nussbaum C, de La Vaissiere R, Noiret A, Jaeggi D, Landrein P, Righini C. Geometry and properties of the excavation induced fractures at the Meuse/Haute-Marne URL drifts. Rock Mech Rock Eng 2014; 47: 21-41.

[10] Armand G, Conil N, Talandier J, Seyedi DM. Fundamental aspects of the hydromechanical behaviour of Callovo-Oxfordian claystone: From experimental studies to model calibration and validation. Computers and Geotechnics 2017; 85: 277–286.

[11] Birkholzer JT, Tsang CF, Bond AE, Hudson JA, Jing L, Stephansson O. 25 years of DECOVALEX - Scientific advances and lessons learned from an international research collaboration in coupled subsurface processes. Int J Rock Mech Min Sci 122 (2019) 103995.

[12] Seyedi DM, Plua C, Vitel M, Armand G, Rutqvist J, Birkholzer J, Xu H, Guo R, Thatcher KE, Bond AE, Wang W, Nagel T, Shao H and Kolditz O. Upscaling THM modelling from small-scale to full-scale in-situ experiments in the Callovo-Oxfordian claystone. Submitted to the Int J Rock Mech Min Sci 2020.

[13] Plua C, Manon V, Seyedi D, Armand G, Rutqvist J, Birkholzer J, Xu H, Guo R, Tatcher KE, Bond AE, Wang W, Nagel T, Shao H, Kolditz O. Decovalex-2019: Task E final report. LBNL-2001265. 2020.

[14] Rutqvist J, Barr D, Datta R, Gens A, Millard A, Olivella S, Tsang CF, Tsang Y. Coupled Thermal–hydrological–mechanical analyses of the Yucca Mountain Drift Scale Test — comparison of field measurements to predictions of four different numerical models. Int J Rock Mech Min Sci 2005; 42: 680–697.

[15] Gens A, Guimaraes L, Garcia-Molina A, Alonso EE. Factors controlling rock-clay buffer interaction in a radioactive waste repository. Engineering Geology 2002; 64: 297-308.

[16] Guo, R., 2011. Thermohydromechanical modelling of the Buffer/Container Experiment. Eng. Geol. 122, 303–315.

[17] Thomas HR, Cleall PJ, Chandler N, Dixon D, Mitchell HP. Water infiltration into a large-scale in-situ experiment in an Underground Research Laboratory. Geotechnique 2003; 53: 207–224.

[18] Nguyen TS, Selvadurai APS, Armand G. Modelling the FEBEX THM experiment using a state surface approach. Int J Rock Mech Min Sci 2005; 42: 639-651.

[19] Guo R, Dixon D, Martino J. Thermohydromechanical modelling of a full-scale tunnel sealing clay bulkhead. Journal of Geotechnical and Geoenvironmental Engineering 2006; 132:12–23.

[20] Bond A, Chittenden N, Thatcher K. RWM coupled process project: first annual report for DECOVALEX-2019. QRS-1612D-R1 v1.2. 2017.

[21] Guo R, Thatcher KE, Seyedi KM, Plua C. Calibration of the thermo-hydro-mechanical parameters of the Callovo-Oxfordian claystone and the modelling of the ALC experiment. Int J Rock Mech Min Sci. 2020. In press.

[22] Acres Consulting Services Limited in conjunction with RE/SPEC Ltd. A feasibility study of the multilevel vault concept. Atomic Energy of Canada Limited Technical Report, TR-297. 1985.

[23] Acres Consulting Services Ltd. A preliminary study of long-hole emplacement alternatives. Atomic Energy of Canada Limited Technical Report, TR-346. 1993.

[24] Baumgartner P, Tran TV, Burgher R. Sensitivity analyses for the thermal response of a nuclear fuel waste disposal vault. Atomic Energy of Canada Limited Technical Report, TR-621, COG-94-258. 1994.

[25] Tsui KK, Tsai A. Thermal analyses for different options of nuclear fuel waste placement. Atomic Energy of Canada Limited Technical Report, AECL-7823. 1985.

[26] Park JH, Kuh JE, Kwon S, Kang CH. Thermal analysis of high level radioactive waste repository using a large model. J. Kor. Nucl. Soc. 2000; 32: 244–253.

[27] Guo R. Numerical modelling of a deep geological repository using the in-floor borehole placement method. Nuclear Waste Management Organization, NWMO TR-2007-14 (Available at www.nwmo.ca). 2007.

[28] Guo R. Sensitivity analyses to investigate the influence of the container spacing and tunnel spacing on the thermal response in a deep geological repository. Nuclear Waste Management Organization, NWMO TR-2008-24 (Available at www.nwmo.ca). 2008.

[29] Verma AK, Gautam P, Singh TN, Bajpai RK. Discrete element modelling of conceptual deep geological repository for high-level nuclear waste disposal. *Arabian Journal of Geosciences* 2015; **8:** 8027–8038.

[30] Abootalebi P,Siemens G. Short-term thermal modelling of a conceptual deep geological repository in Canada. Environmental Geotechnics 2020; 7: 17-31.

[31] Carvalho JL, Zivkovic A. Near-Field and Far-Field Thermal-Mechanical Modelling of a Two-Level Deep Geological Repository for Used Nuclear Fuel in Crystalline Rock - an Update. The 52nd U.S. Rock Mechanics/Geomechanics Symposium, 17-20 Jun. 2018. Seattle, Washington.

[32] Butov RA, Drobyshevsky NI, Moiseenko EV, Tokarev UN. Finite element code FENIA verification and application for 3D modelling of thermal state of radioactive waste deep geological repository. Journal of Physics: Conf. Series 891 (2017) 012174 doi: 10.1088/1742-6596/891/1/012174.

[33] Guo R. Thermal response of a Canadian conceptual deep geological repository in crystalline rock and a method to correct the influence of the near-field adiabatic boundary condition. Engineering Geology 2017; 218: 50-62.

[34] COMSOL. Heat Transfer Module User's Guide. Version: COMSOL 5.4. 2018.

[35] Muller AB, Finley NC, Pearson FJ. Geochemical parameters used in the bedded salt reference repository risk assessment methodology. Sandia National Laboratories Report, SAND81-0557, Albuquerque, NM. 1981.

[36] Andrade ENDAC. The viscosity of liquids. Nature 1930; 125: 309-310.

[37] COMSOL. Structural Mechanics Module User's Guide. Version: COMSOL 5.4. 2018.

[38] Guo R. Prediction of the thermal-hydraulic-mechanical response of a geological responsibility at large scale and sensitivity analyses – DECOVALEX-2019 Task E: Step 4. Nuclear Waste Management Organization. NWMO-TR-2019-12. (Available at www.nwmo.ca). 2019.

[39] Smith DW, Booker JR. Green's functions for a fully coupled thermoporoelastic material. Int J Numerical Analytical Meth Geomechanics 1993; 17:139-163.

[40] Xu H, Rutqvist J, Plúa C, Armand G, Birkholzer J. Modeling of Thermal Pressurization in Tight Claystone using Sequential THM Coupling: Benchmarking and Validation against In-situ Heating Experiments in COx. Tunnelling and Underground Space Technology. (In revision).

Figure 1: Possible architecture of Cigéo, the industrial geological disposal facility

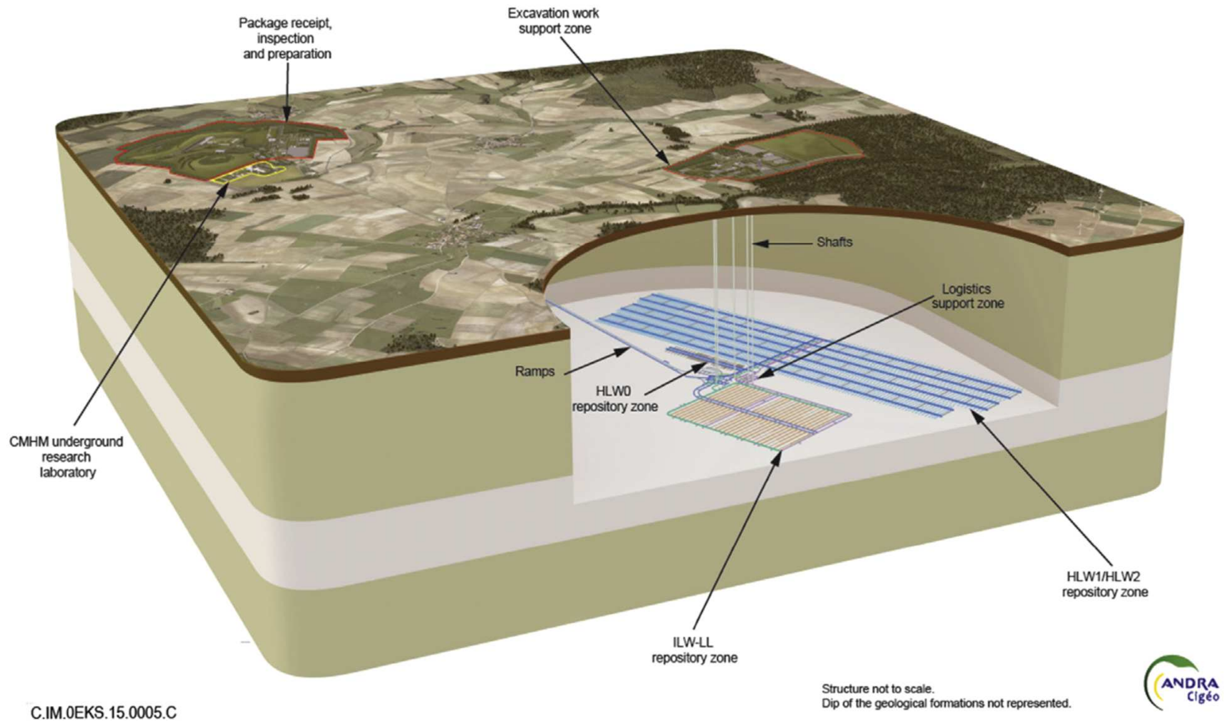

Figure 2: Model geometry of the Base Case with 6 placement cells presented in detail

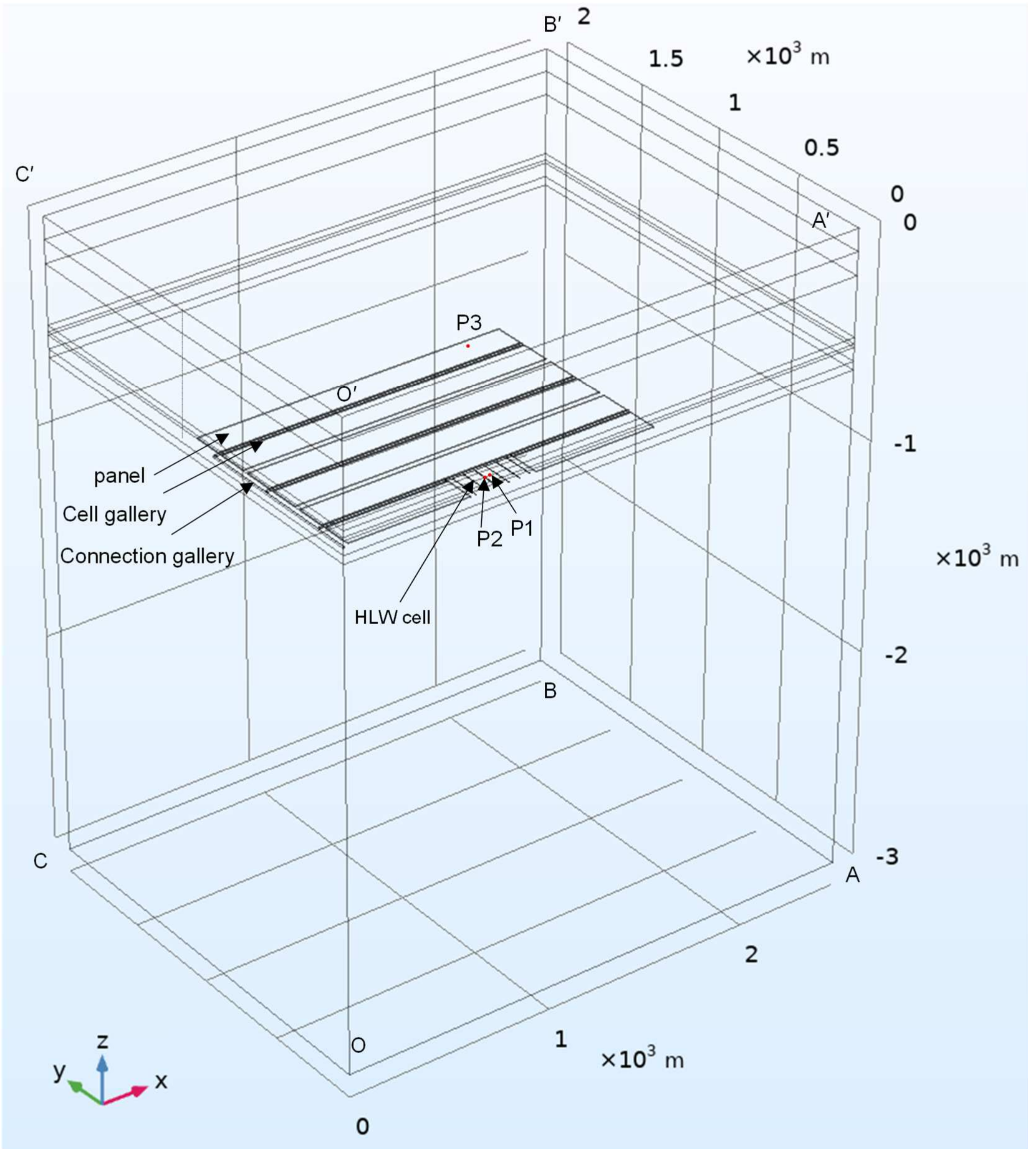

Figure 3: Initial conditions for the THM modelling: (a) Temperature; (b) Pore pressure; and (c) Total stresses

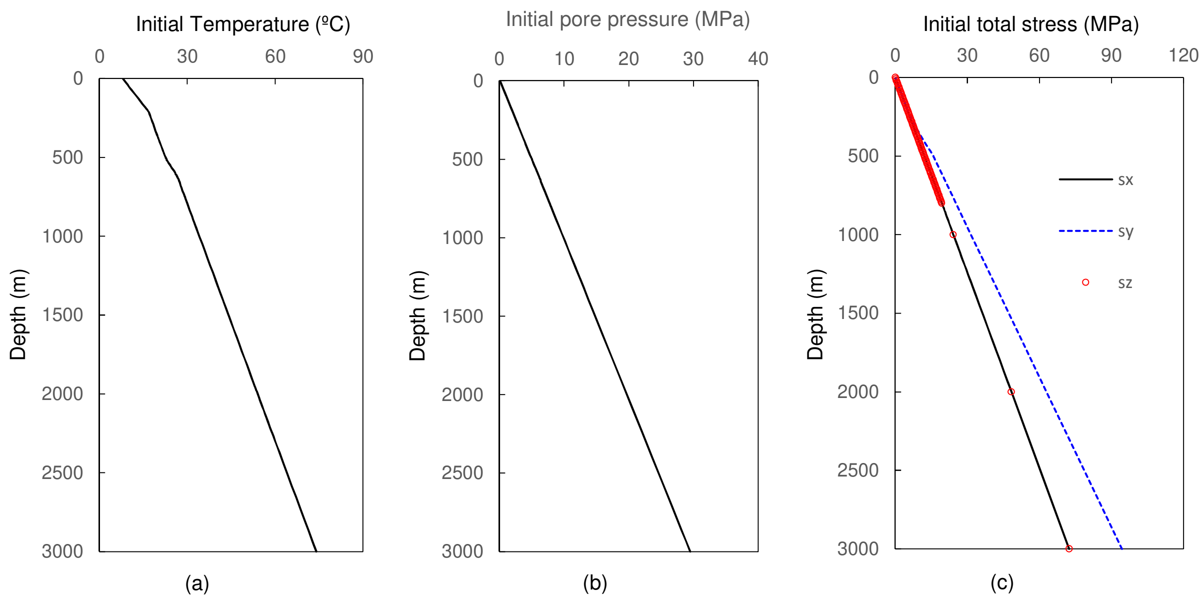

Figure 4: Heat power applied per meter cell with time

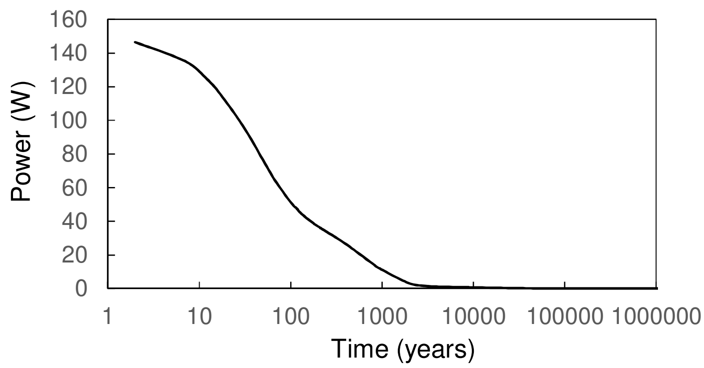

Figure 5: Comparison of simulated temperatures at Points P1 and P2 between 2D model and 3D model

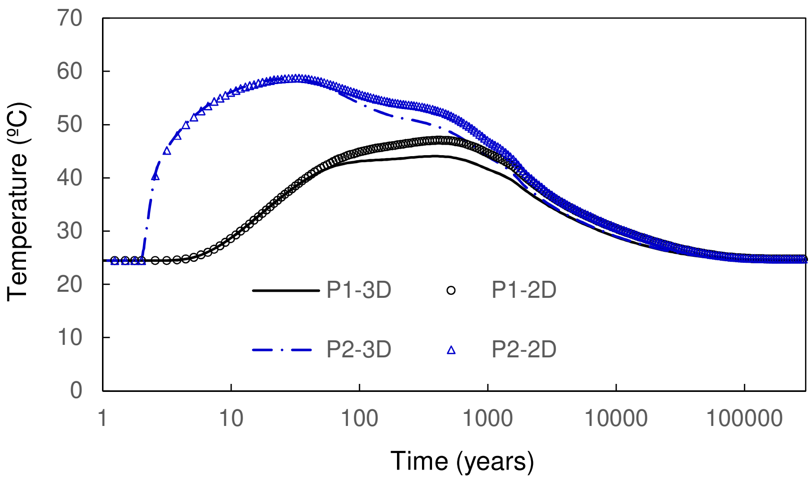

Figure 6: Comparison of simulated pore pressure at Points P1 and P2 between 2D model and 3D model

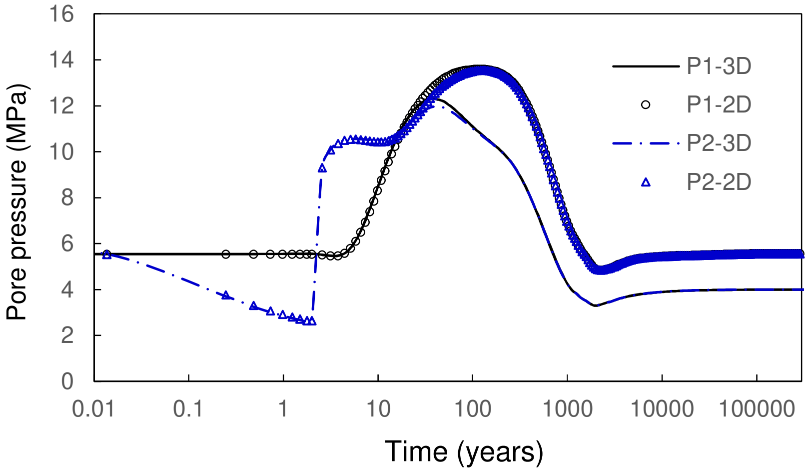

Figure 7: Comparison of simulated uplift at P3 (ground surface above P1) between 2D model and 3D model

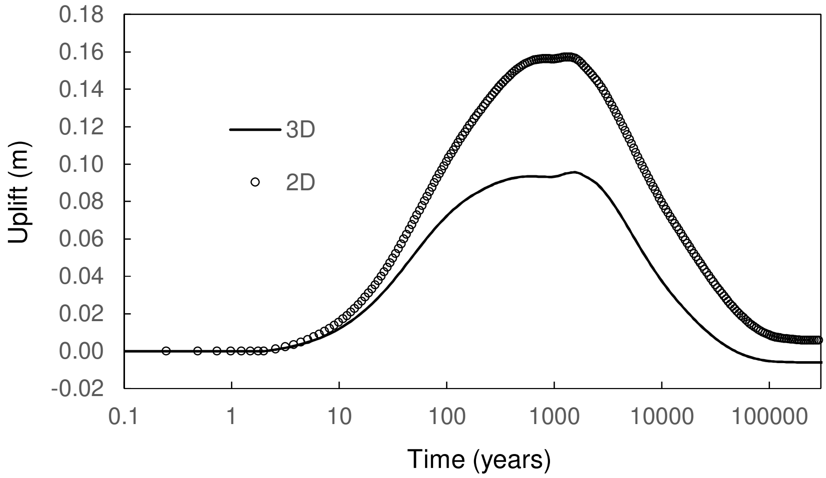

Figure 8: Uplift on the ground surface along Line O′A′ above the repository central line at four different times

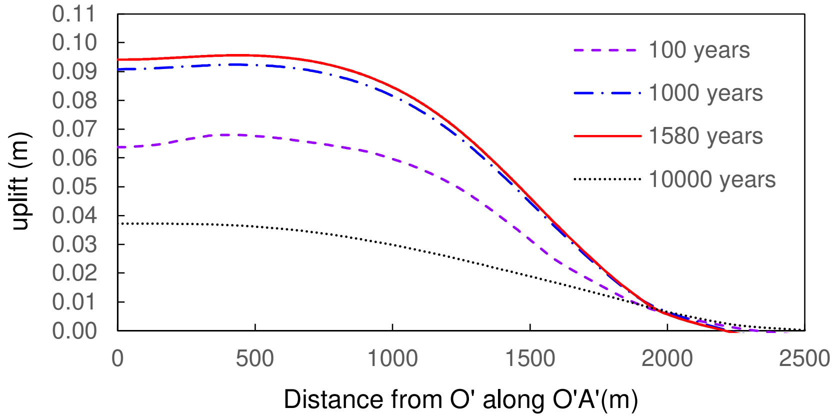

Figure 9: Stresses at Points P1 and P2 (a) in the X-direction and (b) in the Z-direction against time

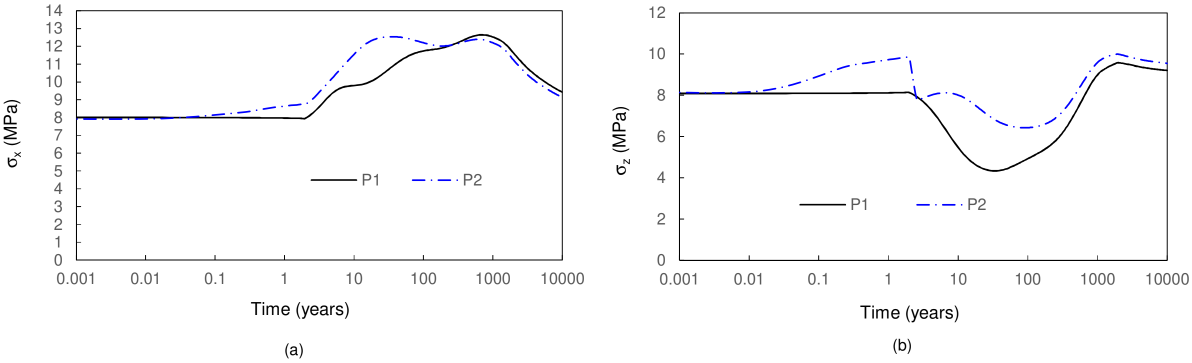

Figure 10: Influence of the number of HLW cells incorporated in detail on (a) temperature and (b) Pore pressure at points P1 and P2.

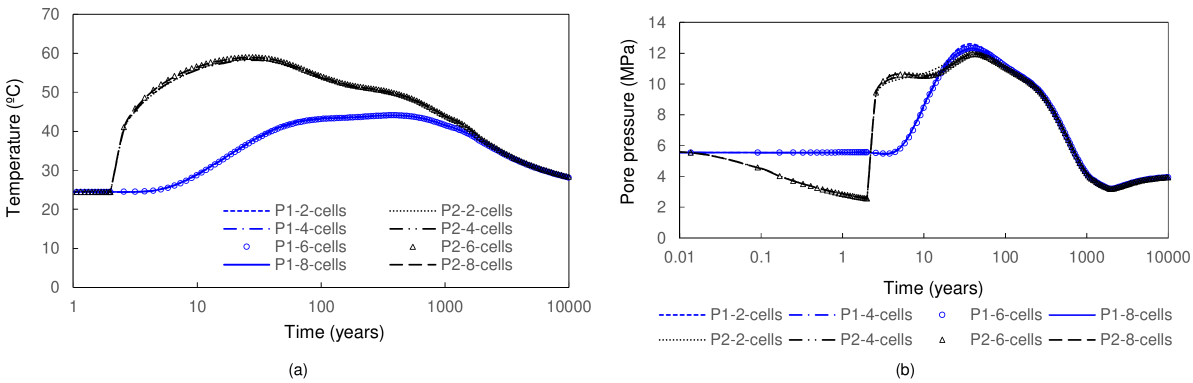

Figure 11: Influence of access/connection tunnels filled with fully-saturated buffer (a) after 2 years and (b) after 1000 years on the pore pressure at Points P1 and P2

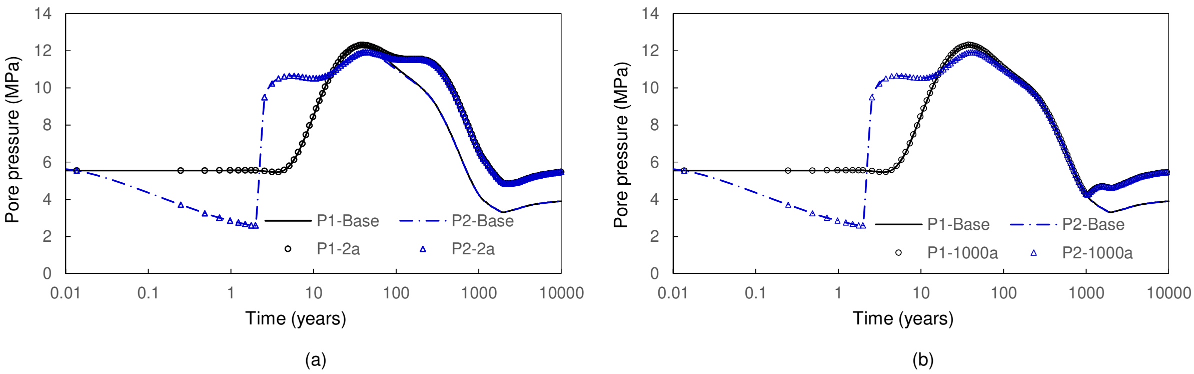

Figure 12: Influence of access/connection tunnels filled with buffer after 2 years and 1000 years on the uplift at Point P3.

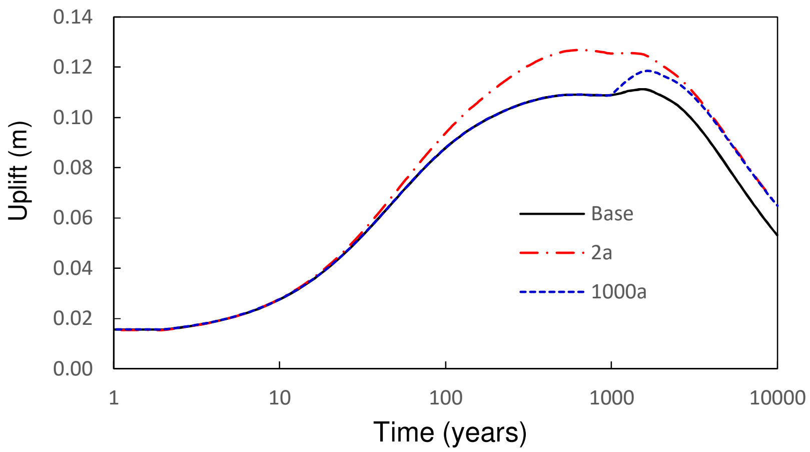

Figure 13: Influence of fixed boundary condition on the HLW cell wall after 2 years on pore pressure at Points P1 and P2

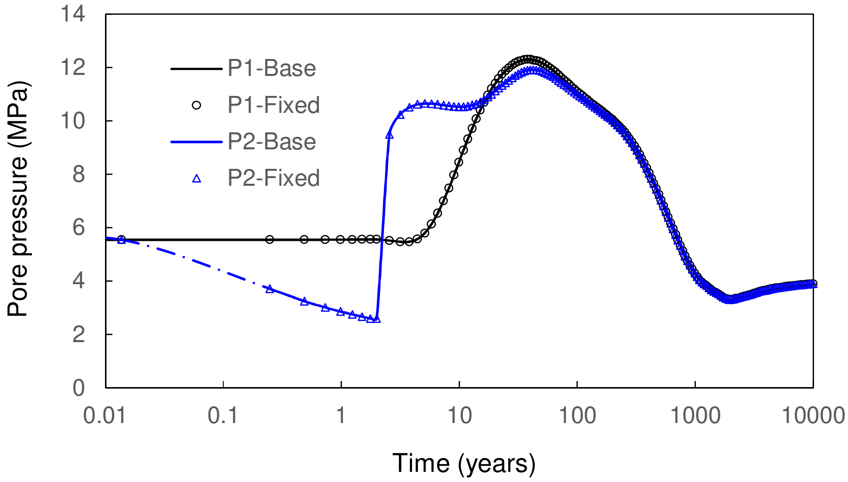

Figure 14: Temperatures at Point P2 from Base Case and cases with minimum values of thermal conductivity, equivalent density or thermal capacity

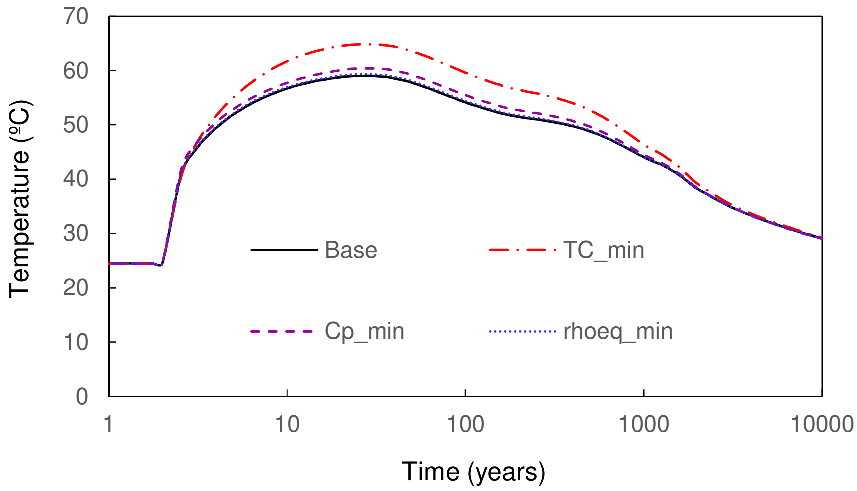

Figure 15: Pore pressure at P2 for the Base Case and cases which cause the pressure to increase

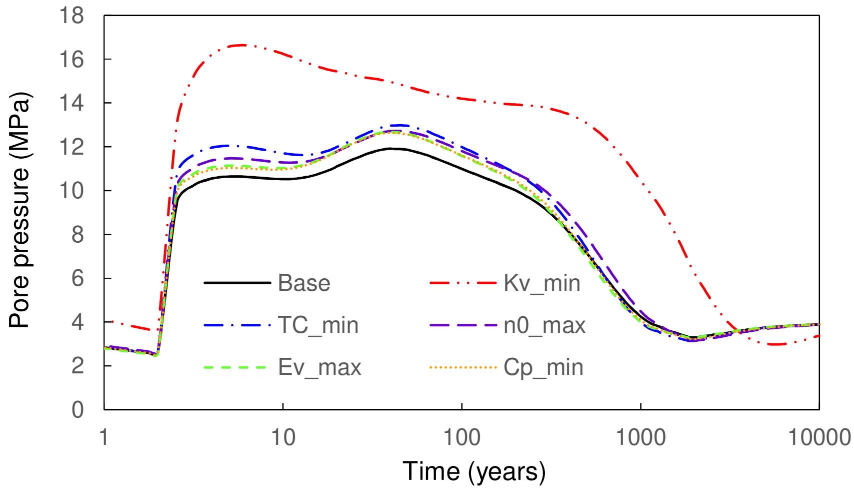

Figure 16: Uplift at Point P3 for the Base Case and cases which cause the ground surface uplift to increase

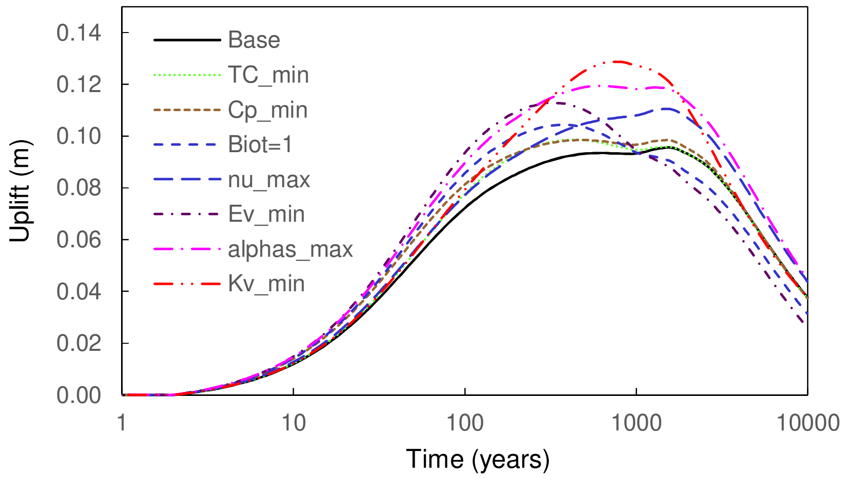

Figure 17: Influence of minimum permeability values of Layer UT, or UA1, or UA23 or USC used on pore pressure at (a) Point P1 and (b) Point P2

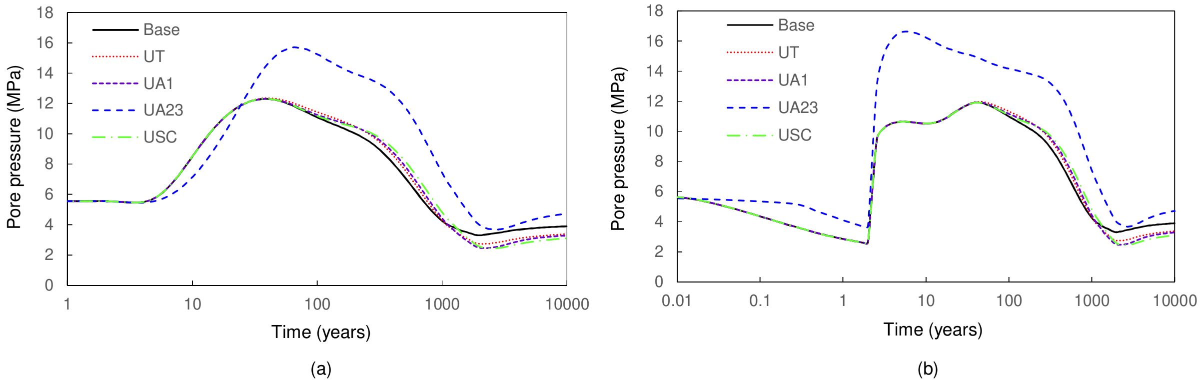

Figure 18: Influence of minimum thermal conductivity values of Layer UT, or UA1, or UA23 or USC used on (a) temperatures and (b) pore pressures at Points P1 and P2

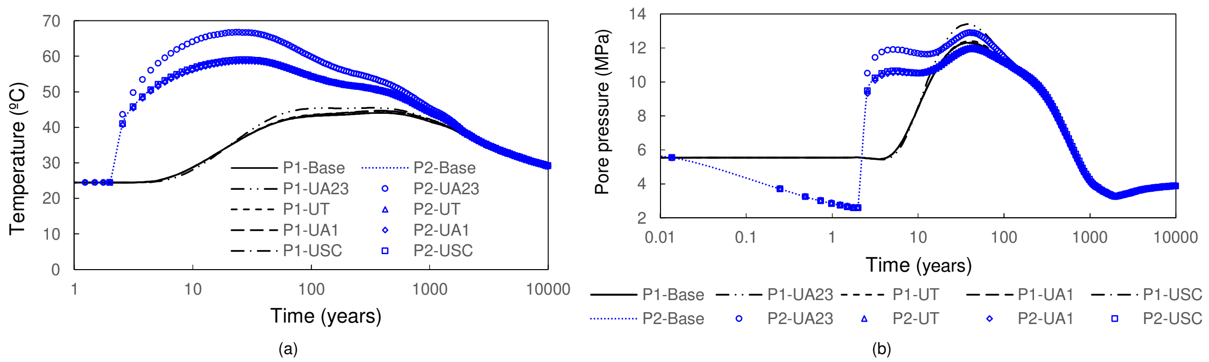

Figure 19: Influence of maximum Young's modulus values of Layer UT, or UA1, or UA23 or USC used on pore pressures at Points P1 and P2

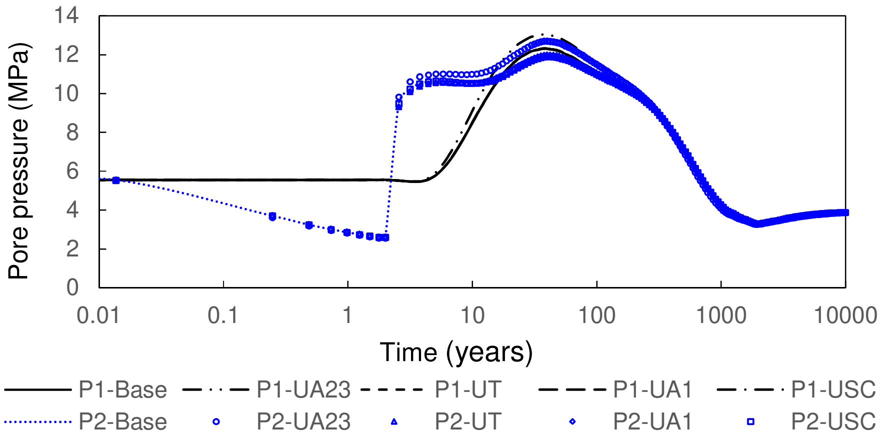

Figure 20: COMSOL point heat source model geometry

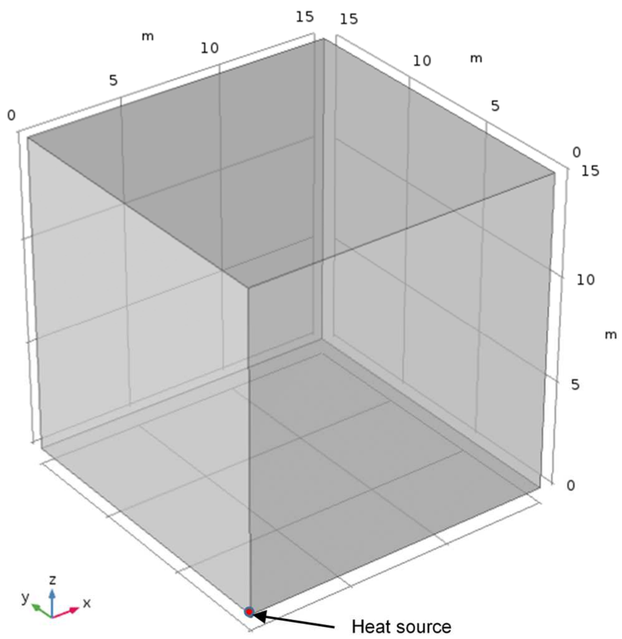

Figure 21: Comparison of the simulated (a) temperatures and (b) pore pressures using COMSOL model with the theoretical solutions at Points Q1, Q2, Q3 and Q4.

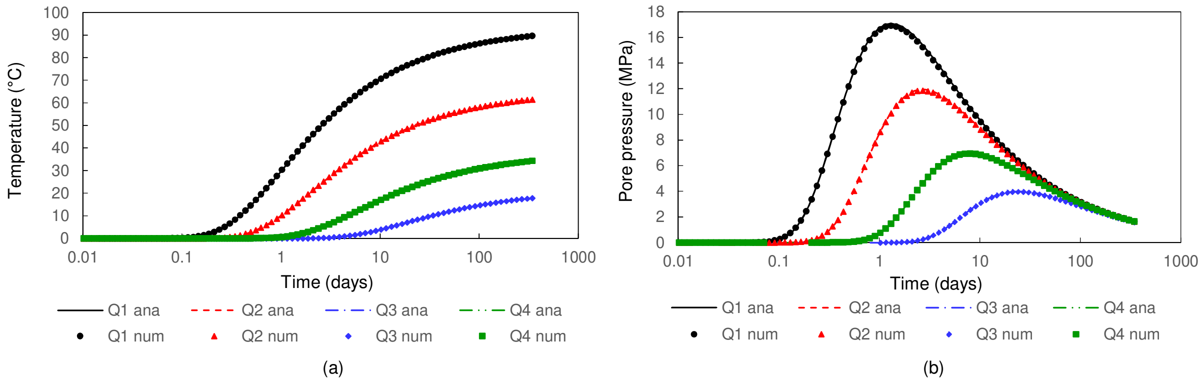

Figure 22: Comparison of the modelled (a) displacements and (b) normal stresses using the COMSOL model with the theoretical solutions at Point Q4.

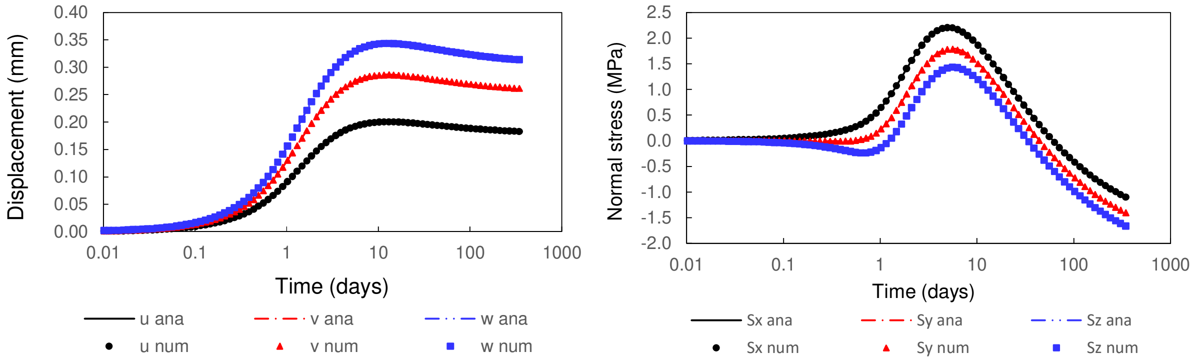


(a) (b)

Figure 23: Comparison of temperatures between the coupled THM COMSOL model and the accurate results at Points P1 and P2

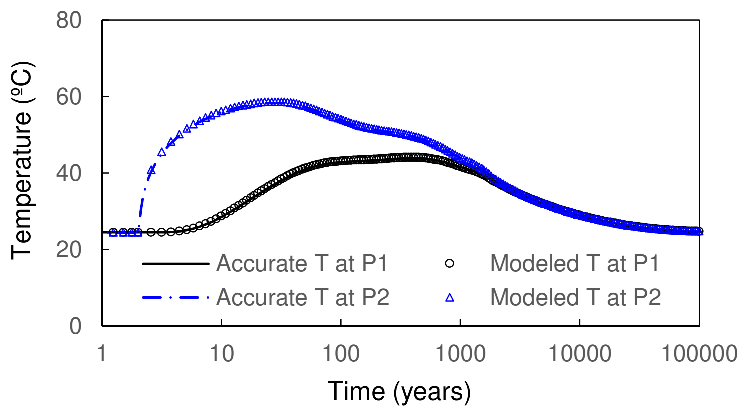

Table 1: Depths of each geological unit considered in the COMSOL model and its thickness

| Formation | | Abbreviation | Depth (m) | Thickness (m) |
|---|---|---|---|---|
| Barrois Limestone | | bar | 0 – 103.4 | 103.4 |
| Kimmeridgian | | kim | 103.4 – 211.4 | 108 |
| Carbonated Oxfordian | | oxf | 211.4 – 488.0 | 276.6 |
| Callovo-Oxfordian | USC | usc | 488.0 – 517.4 | 29.4 |
| | UT | ut | 517.4 – 532.6 | 15.2 |
| | UA23 (UA2-UA3) | ua23 | 532.6 – 595.8 (cells at depth of 560 m) | 63.2 |
| | UA1 | ua1 | 595.8 – 635.0 | 39.2 |
| Dogger | | dog | >635.0 | |

Table 2: Boundary conditions on the HLW cell walls and access tunnel walls for the Base Case

| Time | Boundary condition type | HLW cells | Access tunnels |
|---|---|---|---|
| 0 – 2 years | Thermal | Initial temperature | Initial temperature |
| | Hydraulic | Atmospheric pressure | Atmospheric pressure |
| | Mechanical | Free surface | Free surface |
| 2 – 10000 years | Thermal | Heat power | No flux |
| | Hydraulic | No flux | Atmospheric pressure |
| | Mechanical | Free surface | Free surface |

Table 3: Minimum, mean and maximum values of THM parameters of geological formations

| Layer | | $E_v$ | $v_{hv}$ | b | $\phi_0$ | $k_v$ | $\rho$ | $\lambda_v$ | $\alpha_s$ | $C_p$ |
|---|---|---|---|---|---|---|---|---|---|---|
| | | $10^9$ Pa | | | | $10^{-20}$ m$^2$ | $10^3$ kg/m$^3$ | W/(m·ºC) | $10^{-5}$ ºC$^{-1}$ | J/(kg·ºC) |
| bar | | 3.60 | 0.3 | 0.6 | 0.130 | 10 | 2.45 | 1.10 | 2.20 | 1024 |
| Kim | | 3.60 | 0.3 | 0.6 | 0.130 | 10 | 2.45 | 1.10 | 2.20 | 1024 |
| Oxf | | 330.00 | 0.3 | 0.6 | 0.130 | 10000 | 2.47 | 2.3 | 0.45 | 925 |
| usc | min | 5.50 | 0.2 | 0.6 | 0.097 | 0.26 | 2.42 | 1.29 | 1.00 | 842 |
| | mean | 12.80 | 0.3 | 0.6 | 0.150 | 1.87 | 2.48 | 1.79 | 1.75 | 978 |
| | max | 20.10 | 0.4 | 1.0 | 0.185 | 7.33 | 2.54 | 2.45 | 2.50 | 1114 |
| ut | min | 4.00 | 0.2 | 0.6 | 0.143 | 0.26 | 2.40 | 1.08 | 1.00 | 842 |
| | mean | 8.50 | 0.3 | 0.6 | 0.173 | 1.87 | 2.45 | 1.47 | 1.75 | 978 |
| | max | 12.80 | 0.4 | 1.0 | 0.206 | 7.33 | 2.49 | 1.91 | 2.50 | 1114 |
| ua23 | min | 3.70 | 0.2 | 0.6 | 0.150 | 0.26 | 2.34 | 9.80 | 1.00 | 842 |
| | mean | 7.00 | 0.3 | 0.6 | 0.193 | 1.87 | 2.42 | 1.31 | 1.75 | 978 |
| | max | 10.70 | 0.4 | 1.0 | 0.249 | 7.33 | 2.48 | 1.81 | 2.50 | 1114 |
| ua1 | min | 3.80 | 0.2 | 0.6 | 0.128 | 0.26 | 2.40 | 1.12 | 1.00 | 842 |
| | mean | 12.50 | 0.3 | 0.6 | 0.164 | 1.87 | 2.46 | 1.63 | 1.75 | 978 |
| | max | 21.80 | 0.4 | 1.0 | 0.205 | 7.33 | 2.51 | 2.22 | 2.50 | 1114 |
| dog | | 31.00 | 0.3 | 0.6 | 0.100 | 100 | 2.47 | 2.30 | 0.45 | 925 |

Table 4: Ratios of horizontal to vertical parameters

| | $E_h/E_v$ | $v_h/v_v$ | $k_h/k_v$ | $\lambda_h/\lambda_v$ |
|---|---|---|---|---|
| bar | 1.0 | 1.0 | 1.0 | 1.4 |
| kim | 1.0 | 1.0 | 1.0 | 1.4 |
| oxf | 1.0 | 1.0 | 1.0 | 1.0 |
| usc | 1.5 | 1.0 | 3.0 | 1.0 |
| ut | 1.5 | 1.0 | 3.0 | 1.5 |
| ua23 | 1.5 | 1.0 | 3.0 | 1.5 |
| ua1 | 1.5 | 1.0 | 3.0 | 1.5 |
| dog | 1.0 | 1.0 | 1.0 | 1.0 |

Table 5: THM parameters of the rock used in the analytical solution for validation

| Parameters | Rock | Water |
|---|---|---|
| Initial porosity | 0.15 | NA |
| Equivalent thermal conductivity of rock (W/(m· ºC)) | 1.7 | NA |
| Equivalent density of rock (kg/m$^3$) | 2400 | NA |
| Equivalent heat capacity of rock (J/(kg· ºC)) | 1000 | NA |
| Permeability (m$^2$) | $4.5 \times 10^{-20}$ | NA |
| Young's modulus (MPa) | 4500 | NA |
| Poisson's ratio | 0.3 | NA |
| Rock volumetric thermal expansion (1/ºC) | $4.2 \times 10^{-5}$ | NA |
| Reference density of water (kg/m$^3$) | NA | 1000 |
| Compressibility of water (1/Pa) | NA | 0 |
| Heat capacity of water (J/(kg· ºC)) | NA | 4180 |
| Dynamic viscosity of water (Pa·s) | NA | $1 \times 10^{-3}$ |
| Water volumetric thermal expansion (1/ ºC) | NA | $4 \times 10^{-4}$ |
| Biot coefficient | 0.6 | NA |